ADVANCED FUNCTIONAL MATERIALS
www.afm-journal.de

Preserving the Li {110} Texture to Achieve Long Cycle Life in Li Metal Electrode at High Rates

*Xitao Hu, Yao Gao, Yongming Sun, Zhen Hou, Yufeng Luo, Danni Wang, Jiangpeng Wang, Biao Zhang, Zijian Zheng, and Quan Li**

{110} textured Li metal electrode shows superior cycle performance when compared to its counterparts with other crystallographic textures or no texture. However, at high rates it suffers from a shortened cycle life that becomes significant with large cycling capacities – a common problem for most alkaline metal electrodes. In the present work, the morphological and structural evolution of the texture-dependent Li electrodes cycled at different current densities is investigated and discovered that the cycling current density affected both the morphological and the crystallographic texture evolution of Li {110} metal electrode. In particular, loss of {110} texture at increased current densities accelerated the morphological deterioration of Li, leading to roughened Li plating and loose Li packing, and thus promoting the undesired consumption of Li and electrolyte. Thereafter a low-rate-healing strategy that significantly elongated the cycle life of Li metal electrode cycled at high rates is proposed. By adopting the healing strategy, a Li||Li symmetrical cell cycled at 10 mA cm^{-2} with a capacity of 10 mAh cm^{-2}(with a 50% depth of discharge) can last for >800 runs, and a Li||LFP full cell can run for >300 cycles at 5 C with virtually no capacity degradation compared to the first cycle after activation.

1. Introduction

Achieving long-cycle stability in Li metal remains a major challenge for batteries adopting Li metal anode. The cycling rate is an important parameter in evaluating the cycle stability of the Li metal electrode. As a matter of fact, high-rate cycling is important/desired in many practical applications.[1] Unfortunately, the long-cycle stability of Li metal electrodes at high rates is always found inferior to those running at low ones, especially with large cycling capacities.[2] The inferior cycle performance of Li metal at high rates is commonly ascribed to the more severe fractal growth of Li metal as promoted by the high current density in an electrochemical process, resulting in increased Li dendrite[3] and/or dead Li formation/electrolyte depletion,[4] and thus shortened battery cycle life.[5] In addition, it has also been argued that the solid electrolyte interphase (SEI) formed at high current density is fragile and thus unfavorable.[6]

Existing solutions to tackle the problems incurred at high current densities are general strategies targeting at either restricting the Li dendrite formation or improving the electrolyte interface stability. Representative ones include the employment of three-dimensional (3D) current collectors that reduce the local current density upon electrochemical cycling[7] and thus suppressing the Li dendrite formation, as well as building artificial SEI that protects the Li metal surface[8] from undesired electrode/electrolyte consumption. Despite all efforts, the long-cycle stability of Li metal electrodes at high rates (especially with large capacity) remains unsatisfactory.[9] Recently, texturing of Li metal appears as a new strategy to suppress the non-uniform growth of Li in a battery process and thus improve the cycle life of the respective cells.[10] Theoretical study

X. Hu, Y. Gao, J. Wang, Q. Li
Department of Physics
The Chinese University of Hong Kong
Shatin, New Territories, Hong Kong 999077, China
E-mail: liquan@cuhk.edu.hk

Y. Sun
Wuhan National Laboratory for Optoelectronics
Huazhong University of Science and Technology
Wuhan 430074, China

Z. Hou, D. Wang, B. Zhang
Department of Applied Physics
The Hong Kong Polytechnic University
Kowloon, Hong Kong 999077, China

Y. Luo, Z. Zheng
Laboratory for Advanced Interfacial Materials and Devices
Research Center for Smart Wearable Technology
Institute of Textiles and Clothing
The Hong Kong Polytechnic University
Kowloon, Hong Kong 999077, China

The ORCID identification number(s) for the author(s) of this article can be found under https://doi.org/10.1002/adfm.202307404

DOI: 10.1002/adfm.202307404

suggests that the {110} is the most promising texture as such a plane associates with the lowest surface energy and surface diffusion barrier for Li ions in the practical battery working range, and thus becomes the most reluctant to take the fractal growth pattern when compared to all other crystalline planes of Li.[11] A couple of methods have been found effective in producing the {110} textured Li. Zhao et al. are the first ones to demonstrate the {110} texture of Li by depositing Li at a current density of 1 mA cm^{-2} with a capacity of 20 mAh cm^{-2} on Cu foil, as governed by thermodynamic principles.[10a] Recently we have succeeded in preparing the Li metal foil with {110} texture (denoting as Li {110}) using a simple mechanical method[10b] based on the conventional theory of slip system activation.[12] Most recently, Li et al. have also reported the {110} texture of lithium metal by applying unidirectional pressure on electrochemically deposited Li (with high capacity).[10c] In all these recent reports, exceptional cycle performance has been found in the {110} textured Li electrodes when compared to other Li textures or Li electrodes without specific textures.[10] Unfortunately, the {110} textured Li also suffers from a much shorter cycle life at high current densities, a phenomenon similar to all other Li metal electrodes w/o crystallographic textures.

In this work, we identified factors responsible for the deteriorated cycle performance of Li {110} electrodes at increased current densities by examining the structural/morphological evolution features of the Li {110} electrode cycled at different rates, especially those with large capacities. We showed that the morphological characteristics of the cycled Li electrode were correlated to its starting texture that evolved with cycling. What important is that the cycling current density would affect both the morphological and the texture evolution of the Li metal electrode. On the one hand, the high current density promoted nucleation/growth of Li grains of small size that were more prone to dead Li formation (and electrolyte consumption). On the other hand, the dominance of the Li {110} texture was only maintained at low current densities upon electrochemical cycling. It is important to note that the benefit of using Li {110} lies in its capability of maintaining the surface flatness upon electrochemical cycling, and thus a dense and smooth Li electrode favoured for long cycle life.[10b] Then the loss of the {110} texture at increased current densities accelerated the morphological deterioration of the electrochemically processed Li. In other words, the benefit brought by the {110} texture could not last at high current densities. Based on such knowledge, we developed a low-rate-healing strategy that significantly elongated the cycle life of the Li metal electrode cycling at high rates in both symmetrical and full cells.

2. Results and Discussion

Li {110} electrode showed superior cycle performance over other Li metal electrodes (all without artificial SEI), including the pristine Li (no preferential texture) and Li {100} (Li foil with {100} texture) in both esters[10b] and ether (Figure S1, Supporting Information) electrolytes. In fact, the cycle performance of bare Li {110} is comparable to many lithium metal electrodes with artificial SEI.[13] The superior performance is ascribed to the lowest surface energy and Li-ion diffusion barrier associated with the Li {110} plane that promotes the presence of flat surfaces over rough ones [10a,b] in an electrochemical process and thus is less prone to Li dendrite and/or dead Li accumulation (Figure S2, Supporting Information). Unfortunately, like all other Li metal electrodes w/o texture, the Li {110} also suffered from a decayed cycle performance when running at high current densities. For example, symmetrical cells of Li {110} running at a current density of 1 mA cm^{-2} with a capacity of 1 mAh cm^{-2} lasted for ≈1000 cycles (≈2050 h) but reduced to ≈800 cycles (≈210 h) when running at 10 mA cm^{-2} with the same capacity (Figure S3, Supporting Information). The cycle life decay became significant when the cells were cycled at larger capacities. As shown in **Figure 1**, Figures S4 and S5 (Supporting Information), with the capacity of 5 mAh cm^{-2}, the cycle lives of the symmetrical cells were estimated as ≈580, ≈460, and ≈350 cycles, at current densities of 5, 10 and 20 mA cm^{-2}, respectively.

To find out the critical factors responsible for the reduced cycle life at increased current densities, we first characterized the morphological evolution of the respective electrode surface by scanning electron microscope (SEM). The SEM images of the Li {110} electrode surface after the 1st cycle platting (anode side) and stripping (cathode side) at current densities of 5, 10 and 20 mA cm^{-2} can be found in **Figure 2**a and Figure S6 (Supporting Information), respectively. While no obvious difference was observed in the stripped morphologies of the three samples (Figure S6, Supporting Information), the plated grain size decreased with increasing current density (Figure 2a), being consistent with literature reports.[13] The thickness of the deposited layer with different current densities after the first cycle is very similar.The electrochemically cycled Li grain size remained similar to the starting situation of the respective samples in prolonged cycles (the surface morphologies of the respective sample after 200 cycles were shown in Figure 2b). More SEM results on the surface morphology evolution of the Li {110} electrodes after different numbers of cycles can be found in Figure S7 (Supporting Information). Consistent observation was made by atomic force microscopy (AFM) that disclosed the surface topography (Figure S8, Supporting Information) of the Li {110} electrode after 200 cycles. Cross-sectional SEM images of the same batch of samples (Figure 2a) revealed a similar Li thickness of ≈38 µm after the 1st plating despite the different current densities employed. Together with Li plating characteristics shown in Figure 2a, this result then suggested a difference in interface/surface that will be in contact with the electrolyte in the following electrochemical process within the plated Li—the largest interface in the case of the smallest Li grain size (sample cycled at the highest current density of 20 mA cm^{-2}). The consequence of such difference is manifested in the cross-sectional morphologies of the respective samples—at the end of the 200 cycles, a huge difference was observed in the thickness of the electrochemically cycled Li layer, with the largest thickness of ≈130 µm found in Li {110} electrode cycled at 20 mA cm^{-2} (Figure 2b) (note that without special indication, the starting thickness of all Li foils is ≈100 µm). At the same time, the {110} texture of the Li electrode was also found to change with cycling, with evolving features affected by the cycling current density. The texture evolution of the electrode was examined using X-ray diffraction (XRD), and a quantitative comparison of the respective samples was made using the relative texture percentage P(hkl) (See details in Figure S9, Supporting Information). For cells running at a small current density of 1 mA cm^{-2} (with a capacity of 1 mAh cm^{-2}), the {110} texture

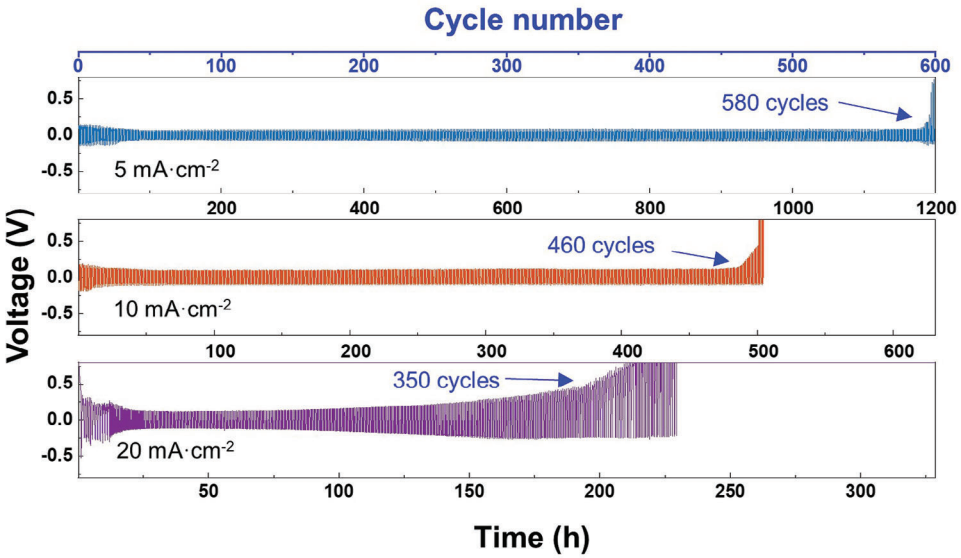

Figure 1. Cycle performance comparison of symmetric cells assembled using Li {110} electrodes (100 µm) cycled at current densities of 5, 10 or 20 mA cm^{-2} with a capacity of 5 mAh cm^{-2} (depth of discharge (DOD) = 25%).

of the Li electrode was found to be dominant toward the end of its cycle life (Figure S9a,b, Supporting Information). As a matter of fact, even if the starting texture of Li is not {110}, cycling at low current density would lead to the increase of {110} texture after a number of cycles (see results of {100} textured Li electrode shown in Figure S9c,d, Supporting Information). One can see a slow decay of P(110) to 60% at the end of 1000 cycles for Li {110} cycled at 1 mA cm^{-2}, while the P(110) increased to more than 40% at the end of 500 cycles for Li {100} cycled at 1 mA cm^{-2}. However, at a larger current density of 10 mA cm^{-2}, loss of {110} texture became significant in Li {110} electrode (Figures S9e,f, Supporting Information)—its P(110) quickly went down to 50% after 400 cycles, and was no longer dominant at the end of cycling (20% at 800 cycles). A similar trend was observed when carbonate ester electrolyte was employed.[10b] The tendency of significant loss of the {110} texture at high current densities was also observed when cells were cycled at a large capacity of 5 mAh cm^{-2}. A comparison of P(110) decay as a function of cycle numbers at different current densities was plotted in Figure 2c (The corresponding XRD data and the P(hkl) evolutions can be found in Figure S10, Supporting Information), in which the most significant {110} texture decay happened at 20 mA cm^{-2}. One point to note is that we did not differentiate between the newly deposited Li and the pre-existing Li in the tests. Instead, we attributed the loss of {110} texture primarily to the electrochemical cycling process, considering the inherent stability of {110} textured Li during storage.[10b] Furthermore, in each cycle, there are irreversible processes that contribute to the depletion of active Li, leading to a gradual disappearance of the original {110} texture. This observation is supported by the cross-sectional SEM images (Figure 2; Figure S2, Supporting Information). Consequently, we conducted the analysis of {110} texture loss based on the entire processed electrode. The texture evolution at different depths of discharge (DOD) was studied using a constant current density of 10 mA cm^{-2} (Figures S11 and S12, Supporting Information). The results show that as the DOD increases from 0.05 (1 mAh cm^{-2}) to 0.5 (10 mAh cm^{-2}), the loss of Li {110} texture becomes more profound. As the cycling current density is identical in these samples, such an increase suggests the contribution from consumption of the initial Li (getting thinner) upon cycling.

The effect of cycling current density on the kinetics of electrochemical processes was evaluated by electrochemical impedance spectroscopy (EIS) and Tafel tests.[14] The obtained Nyquist plots and Tafel plots are shown in Figure S13 (Supporting Information). Fitting the EIS data (Figure S13a,b, Supporting Information) gave the bulk solution resistance (R_s, Figure 2d), SEI resistance (R_{SEI}, Figure 2e) and charge transfer resistance (R_{ct}, Figure 2f). Cells cycled at different current densities had similar R_S values at the 5th cycle and did not change much after 200 cycles. R_{ct} is associated with the Li↔Li$^+$ reaction in the electrode and R_{SEI} represents the capability of Li$^+$ transfer through the SEI.[7b] At the 5th cycle, R_{SEI} and R_{ct} were similar for all cells cycled at different current densities. Both R_{SEI} and R_{ct} were found to increase at the end of 200 cycles for all samples alike. Nonetheless, the most significant increase in both values took place in cells cycled at the highest current density (20 mA cm^{-2}), suggesting a formation of unfavorable SEI in samples cycled at such current density (in comparison with lower current density ones).[15] The exchange current densities were estimated by fitting the linear region of the Tafel plots, as illustrated in Figure S13c,d (Supporting Information). A higher exchange current density would suggest easier depositing/stripping of Li.[16] Specifically, higher exchange current density means that extensive oxidation and reduction reactions occur, which means that Li↔Li$^+$ reactions are more likely to occur on the surface of lithium electrodes.[17] As shown in Figure 2g, the exchange current density at the different rates was similar (≈53.7 mA cm^{-2}) at the 5th cycle. After 200 cycles, the exchange current decreased significantly in all three samples with the most significant decrease occurring in the sample cycled at the highest current density. As suggested by Nagy's work, the {110} plane required the lowest driving force for the electrochemical redox reaction of Li/Li$^+$, associated with the

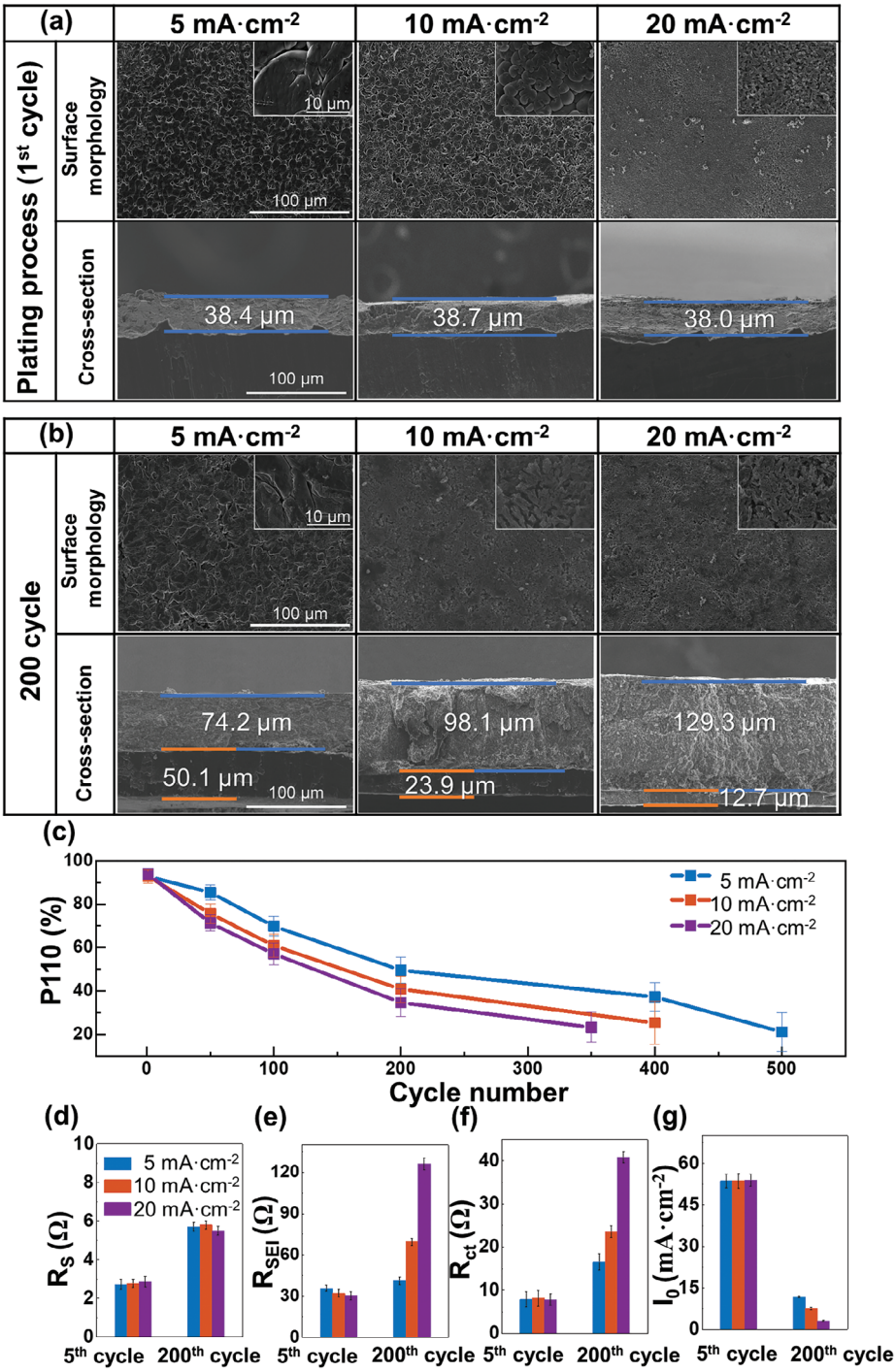

Figure 2. Evolving feature of Li {110} electrodes cycled at current densities of 5, 10 or 20 mA cm^{-2} with a capacity of 5 mAh cm^{-2} a) Surface and cross-section SEM images after 1st plating (anode side) and b) after the 200th cycle (Scalebar of image is 100 μm and scalebar of enlarge image is 10 μm). c) Evolution of the relative texture percentage (P(110)) of the respective samples. d) The bulk solution resistance (R_s), e) SEI resistance (R_{SEI}), f) charge transfer resistance (R_{ct}) and g) the exchange current density (I_0) of the respective samples at the 5th and the 200th cycle.

fastest steady-state nucleation rates among all crystallographic planes.[18] Consequently, when all samples (cycled at different current densities) suffered from the {110} texture loss, a reduction in the respective exchange current densities (I_0) appeared. A most prominent drop in I_0 for the sample running at the highest current density (i.e., 20 mA cm^{-2}) is then consistent with the most significant loss of the {110} texture in such a sample, as suggested by the XRD results.

To find out whether the cycling current density would affect the chemical composition of the SEI formed, X-ray photoelectron

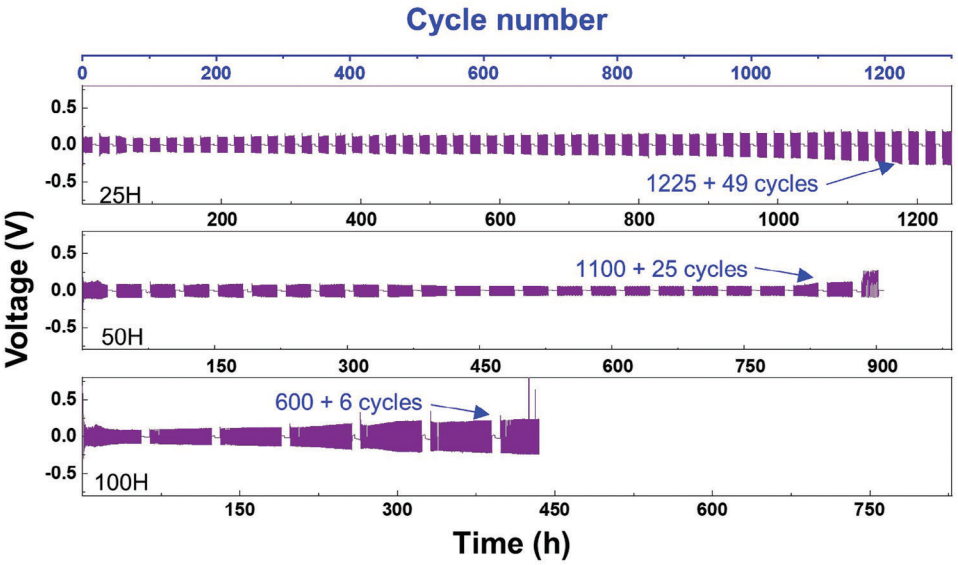

Figure 3. Cycle performance comparison of symmetric cells with Li {110} electrodes (100 µm) at a current density of 20 mA cm^{-2} with a capacity of 5 mAh cm^{-2} (DOD = 25%) with healing cycles (1 mA cm^{-2} with the same capacity) introduced every 25, 50 or 100 cycles.

spectroscopy (XPS) was performed on Li {110} electrodes cycled at current densities of 5, 10 and 20 mA cm^{-2}, with a capacity of 5 mAh cm^{-2}. All Li metal electrodes were examined after the 5th cycle to guarantee adequate SEI formation.[19] The composition of the SEI on Li {110} formed at different current densities is shown in Supplementary Table 1. Very low contents of N, F and S were found (<0.5 at-%) in all samples, and the percentages of Li, C and O were similar. XPS spectra (and their fittings) of the major compositional elements can be found in Figure S14 (Supporting Information), and quantitative analysis is shown in Table S2 (Supporting Information). Again, no obvious difference was identified in samples cycled at different current densities, suggesting that the chemical composition of the SEI did not play a key role in differentiating the cycling performance of cells at different current densities.

We can now discuss the possible effect of cycling current density on the electrochemical performance of Li {110}. First of all, high current density results in a small grain size of the plated Li that is associated with a larger interface with the electrolyte.[20] Considering the unstable interface between the metal Li and the existing electrolytes, this would promote the undesired reactions, consumption of both electrode and electrolyte, and ill SEI formation. This argument is not limited to Li {110}, but is generally applied to Li metal electrodes. Consistent discoveries have indeed been made in the literature.[2,3,8b] It is important to note that the undesired consumption of electrode/electrolyte is expected to be more significant when non-uniform Li plating/stripping takes place. Generally speaking, the non-uniform growth pattern would largely roughen the plated Li surface and lead to loosely packed Li after a certain number of cycles due to damage accumulation (Figure S2, Supporting Information), further deteriorating the electrode/electrolyte interface.[10b] In this regard, Li {110} has a unique advantage as such texture tends to maintain a flat surface in both the stripping and plating processes, and thus a dense Li layer with a smooth surface (Figure S2, Supporting Information). Unfortunately, the loss of Li {110} texture becomes significant at high cycling current densities (Figure 2c). In other words, once the benefit from Li {110} is no longer available, the increased non-uniform Li plating/stripping would aggressively deteriorate the cycle performance of the electrode at high current densities.

Fortunately, we also found that the Li {110} texture can be largely preserved when cells were cycled at a low current density of 1 mA cm^{-2}. This phenomenon is also consistent with a few reports in the literature. For example, Zhao's work showed the electroplated {110} texture was achievable at a low current density in ether electrolyte.[10a] Shi's work also reported that the lithium deposition layer showed strong {110} texture at a small current density (0.1 mA cm^{-2}) in ether electrolyte.[11] The unique property of Li {110} texture inspired a possible solution to improve the cycle life of Li {110} electrode at high current densities, that is, introducing a "healing cycle" that runs at 1 mA cm^{-2} with a certain frequency when the cell is cycled at high current densities. In this way, we hope to demonstrate the importance of {110} presence in cell cycle performance and therein partially recover the decayed {110} texture at each of the healing cycle to improve the cycle life of the cell. **Figure 3** shows the cycle performance of symmetrical cells running at a current density of 20 mA cm^{-2} with a capacity of 5 mAh cm^{-2}, but with healing cycles (1 mA cm^{-2} with the same capacity) introduced every 25, 50 or 100 runs. The corresponding samples are referred to as 25H, 50H and 100H. Improvement in the cycle life has been found in all three samples when compared to the original cell cycled at 20 mA cm^{-2}–5 mAh cm^{-2} (no healing cycle, Figure 1). Specifically, the cycle life of the original cell is found to be improved 3.5 times, 3.1 times and 1.7 times at healing cycle frequencies adopted in samples 25H, 50H, and 100H.

The surface morphologies of the three samples were compared at the 200th cycle and the 201st cycle (right after the healing cycle at a current density of 1 mA cm^{-2} with a capacity of 5 mAh cm^{-2}).

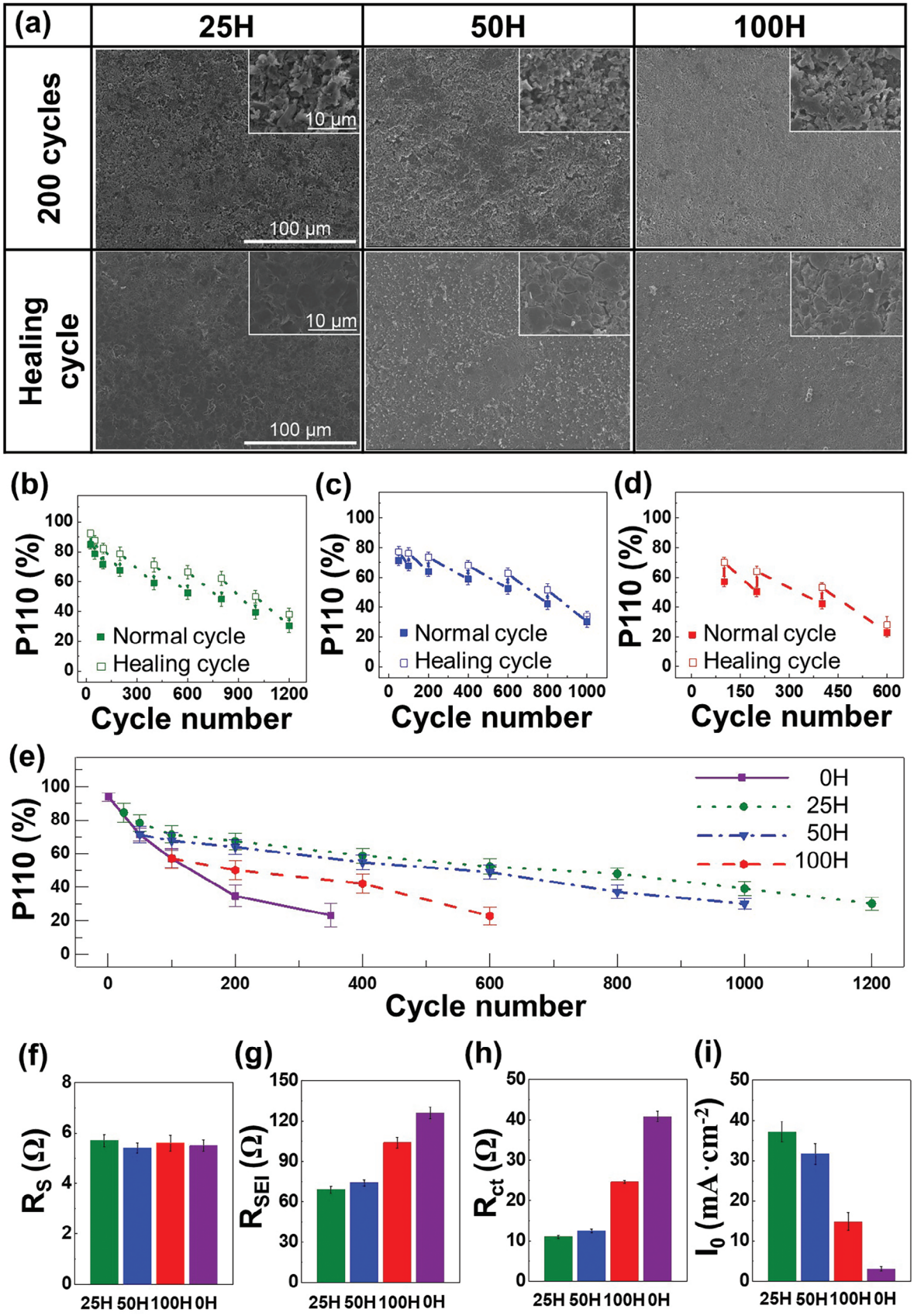

Obvious enlargement on the plated Li grain size and improvement in the surface flatness is found for all three samples after the healing cycle (**Figure** 4a). Surface morphology comparison at a few other cycle numbers can be found in Figure S15 (Supporting Information), where consistent evidence of the healing effect can be observed. On the other hand, the thickness of the electrochemically cycled Li layer decreased with the healing frequency increased (Figure S16, Supporting Information), while a "densification" was found for all healed samples (25H, 50H, and 100H) when compared to the original sample cycled at 20 mA cm^{-2} but without any healing cycles (sample 0H).

As expected, the introduction of the healing cycle was found to partially recover the {110} texture. Ex situ XRD taken from the three samples 25H, 50H, and 100H at different cycle numbers can be found in Figure S17 (Supporting Information). The changes observed in the XRD pattern before and after the healing cycle can be attributed to the deposited lithium rather than the substrate lithium, because the effect of the thickness change of the substrate lithium between the two cycles is negligible. Based on the diffraction intensity, P (110) was calculated and its evolution with cycling was plotted in Figure 4b–d for samples 25H, 50H, and 100H. A comparison of P (110) decay along with cycling w/o the healing cycles is shown in Figure 4 (the healing points were not shown in this figure), when a significant difference was found for the sample with or without the healing cycles. Nevertheless, the "recovering" effect became small when the healing cycle frequency was increased from every 50 cycles to every 25 cycles.

EIS (Figure S18a, Supporting Information) and Tafel (Figure S18b, Supporting Information) tests were carried out after 200 cycles for samples with different healing frequencies (25H, 50H, and 100H). All samples showed similar R_S values (Figure 4f). Both R_{SEI} and R_{ct} were found to increase with the healing frequency decrease (Figure 4g,h). The exchange current densities deduced from the Tafel plots were found to decrease when the healing frequency decreased (Figure 4i). The above results showed that the low current density healing strategy was effective in suppressing the loss of {110} texture when cells were cycled at high rates, and at the same time demonstrated the important role of {110} texture in retaining a flat and dense Li plating in long cycles, reducing the undesired Li and electrolyte consumption. Considering the extent of cycling life improvement and the frequency of healing cycle introduction, we selected the healing frequency used in sample 50H in later experiments unless specified.

This strategy has also been tested in symmetric cells running at different current densities and with different capacities. The current density of the healing cycles was always maintained at 1 mA cm^{-2}. The cells running at a current density of 5 mA cm^{-2} with a capacity of 5 mAh cm^{-2}, the cycle life was improved from ≈580 cycles (Figure 1) to ≈1350 cycles with 27 healing cycles (Figure S19, Supporting Information). When the current density was increased to 10 mA cm^{-2} and capacity increased to 10 mAh cm^{-2} (with 50% DOD), the cycle life was improved from ≈350 cycles (Figure 1) to ≈800 cycles with 16 healing cycles (**Figure** 5a; Figure S20, Supporting Information). The effect of the healing cycle strategy was also tested in full-cell configurations. The full battery uses a non-high load $LiFePO_4$ (LFP, 6.5 mg cm^{-2}) to eliminate the effect of cathode on the full battery performance. The N/P ratio was achieved by using ultra-thin Li {110} metal foil (25 µm). The Li||LFP full cells running at a rate of 5 C lasted for 300 cycles (with 6 healing cycles) and showed negligible capacity reduction (with respect to the capacity of the first cycle after activation at 0.1 C for 3 cycles), in contrast to the sudden cell death at ≈150 cycles when the healing strategy is absent (Figure 5b). The corresponding voltage curves are depicted in Figure S21 (Supporting Information). At the 10th cycle, both cells had not undergone the healing treatment and exhibited similar voltage curves. However, at the 80th cycle, the cell with the healing strategy, which had been healed once, showed a voltage curve that closely resembled that of the 10th cycle. This result demonstrates the successful improvement in cycle stability achieved through the healing strategy. In contrast, the battery without the healing strategy displayed a noticeably deviated voltage curve at the 80th cycle. Additionally, Li||LFP full cells were tested using carbonate-based electrolyte under the same cycle parameters (Figure S22, Supporting Information), and the observed phenomenon was consistent with that observed in the ether electrolyte. The case with the healing strategy exhibited stable operation for more than 450 cycles, while the case without the healing strategy failed at 352 cycles. Li||NCM 811 full cells were also tested to assess the impact of the healing strategy in a high-capacity configuration. The cathode materials NCM 811 exhibited a capacity of ≈5 mAh cm^{-2} at 0.5 C. The Li {110} anode had a thickness of 50 µm. As shown in Figure S23 (Supporting Information), in the case without healing cycles, the initial discharge capacity (after the activation cycles) was recorded as 4.59 mAh cm^{-2}, which gradually decreased to 2.11 mAh cm^{-2} at the 100th cycle at a discharge rate of 0.5 C. Conversely, in the case where the healing cycles were employed, the initial capacity (after the activation cycles) was 4.53 mAh cm^{-2} was comparable, and the capacity retention was 87% (3.96 mAh cm^{-2}) after 100 cycles at 0.5 C. These results demonstrate that the implementation of the healing strategy effectively preserved the capacity of the Li||NCM811 full cells, leading to improved cycle stability.

One shall note that the healing strategy works well for Li metal electrodes with an initial texture of {110}. However, if the starting texture is not {110}, some improvement on the electrode's cycle life can also be obtained, as the healing strategy still helps to enlarge the plated Li grain size and therefore limit the undesired electrode/electrolyte reactions to some extent. Nevertheless, achieving a dominant {110} texture using the healing strategy

Figure 4. Structural and electrochemical feature comparison of Li {110} electrode cycled at a current density of 20 mA cm^{-2} and a capacity of 5 mAh cm^{-2} with different healing cycle frequencies (25H, 50H, 100H refer to samples with healing cycle introduced every 25, 50, or 100 cycles, 0H refers to sample without healing cycle. Scalebar of image is 100 µm and scalebar of enlarge image is 10 µm). a) Top view and cross-sectional SEM images taken from the respective samples after the 200th cycle and after 200 + 1 healing cycle. The relative texture percentage P(110) evolution of b)25H, c)50H, and d)100H. e) Comparison of P(110) evolution of sample 0H, 25H, 50H, and 100H without plotting the healing cycle data in the latter three. f) The bulk solution resistance (R_S), g) SEI resistance (R_{SEI}) and h) charge transfer resistance (R_{ct}).and i) the exchange current density (I_0) of the respective samples after 200th cycle.

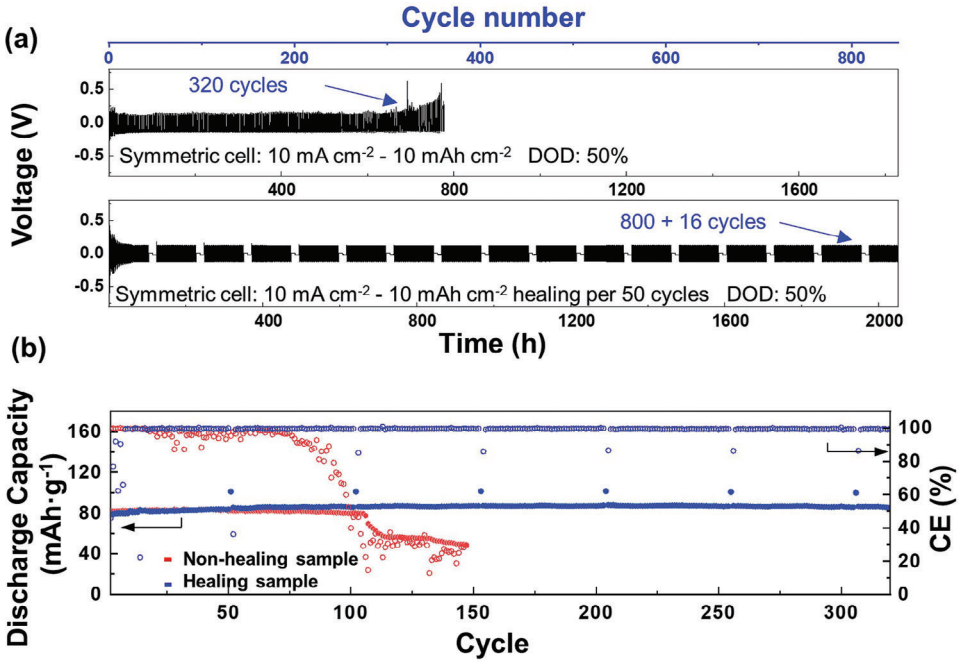

Figure 5. a) Symmetric cell with Li {110} electrode (100 μm) running at a current density of 10 mA cm^{-2} with a capacity of 10 mAh cm^{-2} (DOD = 50%) with and without the healing cycle (introduced every 50 cycles at current density of 1 mA cm^{-2} with a capacity of 10 mAh cm^{-2}). b) Cycling performances of the full cell with Li{110} anode (25 μm) and LFP (mass loading of 6.5 mg cm^{-2}) at 5 C with healing cycle introduced every 50 cycles at 1 C.

is not likely (when the starting one is not), so that the improvement will be limited. Here we show the results of symmetrical Li cells with Li {100} electrodes running at a current density of 20 mA cm^{-2} with a capacity of 5 mAh cm^{-2}, and the healing cycle took place every 25 cycles. The cycle life was improved from ≈80 to ≈150 cycles with 6 healing cycles (Figure S24, Supporting Information). As expected, dominance of {100} texture was found with or without the introduction of the healing cycles (Figure S25, Supporting Information). The morphological evolution of the respective samples is shown in Figure S26 (Supporting Information). The case with pristine lithium foil showed the same phenomenon as the Li {100} symmetric cell (Figure S27, Supporting Information). This again supports the argument that the {110} texture is important for the healing strategy.

3. Conclusion

In summary, we have shown that the long-cycle morphological characteristic of the Li metal electrode depended on its initial crystallographic texture. The {110} texture was associated with the smoothest and densest plating of Li, being beneficial for long-cycle stability. High cycling current density led to Li plating with small grain size that is vulnerable to undesired reaction between the electrode and the electrolyte—a general issue for all Li metal electrodes irrespective of their initial crystallographic texture. This detrimental effect is amplified at high cycling capacity when damage accumulates. A special issue for Li {110} electrode is the quick loss of {110} texture occurring at high-current-density cycling, leading to accelerated deterioration in the morphology of the electrochemically cycled Li, causing shortened cycle life at high rates. These discoveries led to a low-rate-healing strategy that largely preserved the {110} texture when cells were cycled at high rates, thus significantly improving the cell cycle life. The low-rate-healing strategy is developed based on that the lithium {110} crystallographic plane has the lowest crystal plane energy in the battery working environment.[21] This means under thermodynamic control, such as at a low current density, the plating lithium layer tends to expose {110} crystallographic plane.[11,22] The present work revealed the linkage among the Li crystallographic texture, its morphology upon electrochemical cycling, and the cycling rate, when the importance of preserving the {110} texture for long cycle stability is demonstrated.

4. Experimental Section

Texture Formation of Li Metal Foil: To prepare Li foils of {110} texturing, the pristine Li foil (450 μm, China Energy Lithium Co., LTD) was pre-rolled at room temperature using a stainless-steel shaft. The surface of Li foil was then scraped in a uni-directional manner. After that, the lithium foil was further rolled using the same stainless-steel shaft at 75 °C to 100, 50, or 25 μm, respectively. Such a sample was denoted as Li {110}. To prepare Li foils of {100} surface crystallographic orientation, a pristine Li foil of the same size was pressed at 5 MPa for a few seconds to 100 μm by a hydraulic press at room temperature. Such a sample was denoted as Li {100}.

Chemical Polishing of Li Foil Electrodes: Unless otherwise specified, the thickness of Li {110} and pristine lithium foil was 100 and 450 μm, respectively. The thickness of Li {110} is 50 and 25 μm for NCM and LFP full cells respectively. Lithium foils were chemically polished first using a tetrahydrofuran solution of Naphthalene (0.192 g Naphthalene crystal (>99.5%, Sigma Aldrich) dissolved in 15 ml anhydrous tetrahydrofuran (>99.8%, Sigma Aldrich) for 2 min. After that the Li foils were rinsed by 1,3-Dioxolane (DOL) (>99.8%, Sigma Aldrich) a few times to remove the

polishing chemicals. All procedures were carried out in a glove box with oxygen and water content below 0.5 ppm.

Measurements of Performance of Symmetric Cells: CR2032 coin-type cells were assembled to investigate the electrochemical performance of Li foil with specific texturing. Symmetric cells were prepared using lithium foils with the same surface crystallographic orientation (i.e., {100} or {110}). 1 M lithium bis(trifluoromethanesulfonyl)imide (LiTFSI) (anhydrous, Sigma Aldrich) in 1:1 1,2-Dimethoxyethane (DME) (>99.8%, Sigma Aldrich)/DOL solvents with 1% $LiNO_3$ (anhydrous, Sigma Aldrich) were adopted as the electrolyte. 60 µL liquid electrolyte was used for symmetric cell test. At different cycle numbers, the cells were stopped and disassembled. The disassembled electrodes were rinsed by DOL a few times to remove the electrolyte. Then they were sent to ex situ XRD experiments for investigation of crystallographic evolution, or transferred to the SEM for surface morphology inspection of the Li foil along with cycling.

Measurements of Performances Li||LiFePO$_4$ Batteries: Standard CR2032 coin-type cells were also employed for Li||$LiFePO_4$ (LFP) full cells. Each coin cell was filled with 60 µL of liquid electrolyte. The cathode was prepared by mixing the LFP active material (Sigma Aldrich), carbon black and PVDF at the weight ratio of 8: 1: 1 in NMP and casting the formed slurry on the aluminum foil with LFP mass loading of 6.5 mg cm^{-2} in the cathode. The cells were pre-cycled at 0.1 C for three rounds to activate the cathode. After that, they were cycled in a voltage range of 2.4–4.0 V versus Li^+/Li in ether electrolyte. The ester electrolyte of Li||LFP full cells was 1 M lithium hexafluorophosphate ($LiPF_6$, anhydrous, Sigma Aldrich) solution in a mixture of ethylene carbonate (EC, >99.8%, Sigma Aldrich) and diethyl carbonate (DEC, >99.8%, Sigma Aldrich) in a 1:1 volume ratio. The Li||LFP full cells in ester electrolyte were cycled within a voltage range of 2.4–4.3 V versus Li^+/Li.

Characterizations: Galvanostatic cycling and full-cell performance were examined on LANHE CT2001A battery testing system (LAND Electronics). The XRD test was conducted on a Rigaku SmartLab diffractometer (Cu Kα radiation) at 40 kV, 40 mA with a scan rate of 5° min^{-1} and a testing area of 10×10 mm^2. The sample was loaded onto a special holder with a Kapton window in the glove box. SEM images were taken with a JSM 7800F scanning electron microscope at an acceleration voltage of 5 kV. The samples were transferred by a homemade vacuum chamber from the glove box to the microscope to avoid exposure to air. AFM images were obtained with Dimension icon AFM (Bruker) in the glove box. Al Ka X-ray line was used byXPS (Nexsa). EIS and Tafel measurements for symmetric cells were performed using the CHI 760E electrochemical workstation at room temperature. EIS was tested with a frequency range from 10^{-2} to 10^5 Hz with an amplitude of 5 mV. Tafel measurement was measurement with a voltage ranging from −0.4 to 0.4 V with a scan rate of 1 mV S^{-1}.

Supporting Information

Supporting Information is available from the Wiley Online Library or from the author.

Acknowledgements

X.H and Y.G. contributed equally to this work. This work was supported by CUHK direct grant under project no. 4053530.

Conflict of Interest

The authors declare no conflict of interest.

Data Availability Statement

The data that support the findings of this study are available from the corresponding author upon reasonable request.

Keywords

healing strategy, high rates, lithium metal anode, texture

Received: June 29, 2023
Revised: November 9, 2023
Published online: December 2, 2023

[1] Q. Chen, Y. Wei, X. Zhang, Z. Yang, F. Wang, W. Liu, J. Zuo, X. Gu, Y. Yao, X. Wang, F. Zhao, S. Yang, Y. Gong, *Adv. Energy Mater.* **2022**, *12*, 2200072.
[2] a) C. Chen, Q. Liang, Z. Chen, W. Zhu, Z. Wang, Y. Li, X. Wu, X. Xiong, *Angew Chem Int Ed Engl* **2021**,*133*, 26922; b) S. Jiao, J. Zheng, Q. Li, X. Li, M. H. Engelhard, R. Cao, J.-G. Zhang, W. Xu, *Joule* **2018**, *1*, 110.
[3] P. Shi, X.-B. Cheng, T. Li, R. Zhang, H. Liu, C. Yan, X.-Q. Zhang, J.-Q. Huang, Q. Zhang, *Adv. Mater.* **2019**, *37*, 1902785.
[4] J.-N. Chazalviel, *Phys Rev A* **1990**, *42*, 7355.
[5] X. Zhang, A. Wang, X. Liu, J. Luo, *Acc. Chem. Res.* **2019**, *52*, 3223.
[6] J. Sun, J. Peng, T. Ring, L. Whittaker-Brooks, J. Zhu, D. Fraggedakis, J. Niu, T. Gao, F. Wang, *Energy Environ. Sci.* **2022**, *15*, 5284.
[7] a) S. Jin, Y. Jiang, H. Ji, Y. Yu, *Adv. Mater.* **2018**, *30*, 1802014; b) Y. Zhang, W. Luo, C. Wang, Y. Li, C. Chen, J. Song, J. Dai, E. M. Hitz, S. Xu, C. Yang, Y. Wang, L. Hu, *Proc. Natl. Acad. Sci. U. S. A.* **2017**, *114*, 3584; c) J. Zhang, H. Chen, M. Wen, K. Shen, Q. Chen, G. Hou, Y. Tang, *Adv. Funct. Mater.* **2022**, *32*, 2110110.
[8] a) C. Niu, D. Liu, J. A. Lochala, C. S. Anderson, X. Cao, M. E. Gross, W. Xu, J.-G. Zhang, M. S. Whittingham, J. Xiao, J. Liu, *Nat. Energy* **2021**, *5*, 723; b) Q. Yang, J. Hu, Z. Yao, J. Liu, C. Li, *Adv. Funct. Mater.* **2023**, *33*, 2206778.
[9] C. Chen, Q. Liang, G. Wang, D. Liu, X. Xiong, *Adv. Funct. Mater.* **2022**, *32*, 2107249.
[10] a) Q. Zhao, Y. Deng, N. W. Utomo, J. Zheng, P. Biswal, J. Yin, L. A. Archer, *Nat. Commun.* **2021**, *12*, 6034; b) X. Hu, Y. Gao, B. Zhang, L. Shi, Q. Li, *EcoMat* **2022**, *4*, e12264; c) X. Li, C. Chen, Z. Fu, J. Wang, C. Hu, *Energy Stor. Mater.* **2023**, *58*, 155.
[11] F. Shi, A. Pei, A. Vailionis, J. Xie, B. Liu, J. Zhao, Y. Gong, Y. Cui, *USA* **2017**, *114*, 12138.
[12] F. A. R. Al-Salehi, T. C. Firbank, P. R. Lancaster, *Int J Mech Sci* **1973**,*15*, 693.
[13] a) D. T. Boyle, X. Kong, A. Pei, P. E. Rudnicki, F. Shi, W. Huang, Z. Bao, J. Qin, Y. Cui, *ACS Energy Lett.* **2020**, *5*, 701; b) W. Guo, Q. Han, J. Jiao, W. Wu, X. Zhu, Z. Chen, Y. Zhao, *Angew. Chem., Int. Ed.* **2021**, *133*, 7343.
[14] Y. Zhong, P. Huang, W. Yan, Z. Su, C. Sun, Y. Xing, C. Lai, *Adv. Funct. Mater.* **2022**, *32*, 2110347.
[15] J. Takeyoshi, N. Kobori, K. Kanamura, *Electrochemistry* **2020**, *88*, 540.
[16] A. Pei, G. Zheng, F. Shi, Y. Li, Y. Cui, *Nano Lett.* **2017**, *17*, 1132.
[17] X. Xu, X. Jiao, O. O. Kapitanova, J. Wang, V. S. Volkov, Y. Liu, S. Xiong, *Adv. Energy Mater.* **2022**, *12*, 2200244.
[18] K. S. Nagy, S. Kazemiabnavi, K. Thornton, D. J. Siegel, *ACS Appl. Mater. Interfaces* **2019**, *11*, 7954.
[19] L. Wang, A. Menakath, F. Han, Y. Wang, P. Y. Zavalij, K. J. Gaskell, O. Borodin, D. Iuga, S. P. Brown, C. Wang, K. Xu, B. W. Eichhorn, *Nat. Chem.* **2019**, *11*, 789.
[20] X. Liu, Y. Li, L. Zeng, X. Li, N. Chen, S. Bai, H. He, Q. Wang, C. Zhang, *Adv. Mater.* **2022**, *34*, 2108327.
[21] A. Hagopian, M.-L. Doublet, J.-S. Filhol, *Energy Environ. Sci.* **2020**, *13*, 5186.
[22] Y. Li, Y. Li, A. Pei, K. Yan, Y. Sun, C.-L. Wu, L.-M. Joubert, R. Chin, A. L. Koh, Y. Yu, J. Perrino, B. Butz, S. Chu, Y. Cui, *Science* **2017**, *358*, 506.